

Intracellular Delivery of Gold Nanocolloids Promoted by a Chemically Conjugated Anticancer Peptide

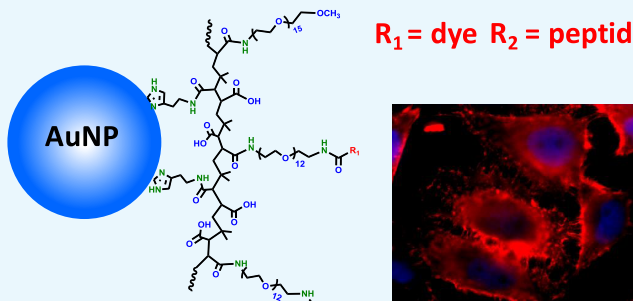
Anshika Kapur,[†] Scott H. Medina,^{‡,§,ID} Wentao Wang,^{†,||,ID} Goutam Palui,[†] Joel P. Schneider,[‡] and Hedi Mattoussi,^{*,†,ID}

[†]Department of Chemistry and Biochemistry, Florida State University, Tallahassee, Florida 32306, United States

[‡]Center for Cancer Research, National Cancer Institute, Frederick, Maryland 21702-1201, United States

Supporting Information

ABSTRACT: We report on the ability of a chemically synthesized anticancer peptide, SVS-1, to promote the rapid uptake of gold nanorods (AuNRs) and gold nanoparticles (AuNPs) by live HeLa cells. For this, AuNPs and AuNRs, surface ligated with a multicoordinating polymer that presents several amine groups per ligand, are simultaneously reacted with SVS-1 and Texas-Red dye; the latter allows fluorescence visualization of the nanocrystals. Using epifluorescence microscopy, we find that incubation of the SVS-1-conjugated AuNPs and AuNRs with a model cancer cell line yields extended staining throughout the cell cytoplasm, even at low conjugate concentrations (~ 0.1 nM). Furthermore, uptake is specific to the SVS-1-conjugated nanocrystals. Additional endocytosis inhibition experiments, where cells have been incubated with the conjugates at 4°C or in the presence of endocytic inhibitors, show that significant levels of conjugate uptake persist. These results combined indicate an uptake mechanism that does not necessarily rely on endocytosis, a promising finding with implications for the use of nanomaterials in the field of biology and nanomedicine.



INTRODUCTION

Over the past two decades bottom-up solution phase growth has allowed researchers access to a wide range of colloidal nanostructures made of homogeneous noble metal cores, with great control over size, shape, and stoichiometry.^{1–5} The designed nanocolloids also feature several unique photophysical and chemical properties not shared by their bulk parent materials, or at the molecular scale.^{4,5} One of the most attractive characteristics of gold nanomaterials is the size- and shape-dependent localized surface plasmon resonance absorption.^{2,6,7} This endows them with enhanced light absorption, which can be tuned from the visible to the near infrared region of the optical spectrum, along with strong light-scattering properties.^{7–9} These characteristics have motivated several groups to integrate these materials in biomedical applications.^{4,9–17} For instance, the strong optical absorption followed by nonradiative energy dissipation exhibited by gold nanocolloids has been exploited to develop them as platforms for photothermal therapy.^{4,18–20} Furthermore, the inertness of the core material, ease of surface functionalization, and low cytotoxicity have been exploited to design and fabricate nanocarriers for therapeutic delivery, including drugs and nucleic acids.^{21,22} Gold nanocolloids have also been actively explored in an array of additional applications ranging from dark field microscopy to optical coherence and photoacoustic tomography imaging.^{23–26}

Use of these nanomaterials for in vivo applications requires access to effective means for delivering them efficiently into live cells and tissues.^{27–29} Intracellular uptake has been investigated in several studies, where groups have explored several receptor-mediated internalization strategies. A number of cell penetrating, often arginine-rich, peptides (CPPs) have been investigated as vehicles to promote the cellular uptake of nanocolloids. These peptides have primarily been derived from the proteins of various viruses, including SV40 large T and HIV 1 TAT protein.^{30,31} However, most if not all those studies have shown that uptake of the CPP-coupled nanocolloids (e.g., luminescent quantum dots, gold as well as other inorganic cores) is primarily controlled by endocytic uptake mechanisms, with internalization efficiency being affected by properties, such as colloid size, structure of the CPP and type of cells used. Researchers have also wrestled with issues ranging from inefficient intracellular uptake to dominance of endocytosis, which tends to yield platforms that are sequestered inside vesicles within mammalian cells.^{32,33} Indeed, most of those studies reported that nanoparticles (NPs) functionalized with arginine-rich peptides or biomolecules like transferrin, herceptin antibody, and folic acid were taken up by cells via endocytosis.^{28,30,34} Overall, homogeneous delivery of NP

Received: September 4, 2018

Accepted: September 14, 2018

Published: October 8, 2018

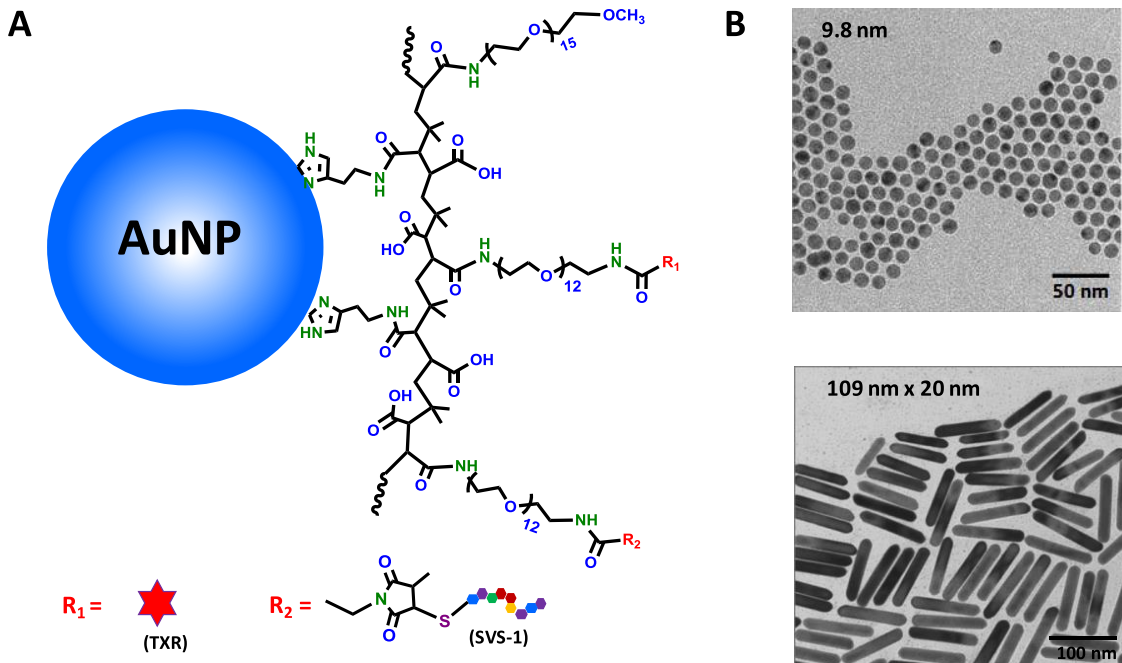


Figure 1. (A) Schematic representation of AuNR-SVS-1/TXR and AuNP-SVS-1/TXR conjugates; an expansion of the structure of the His-PIMA-PEG-SVS-1/TXR is shown. (B) TEM images of AuNPs and AuNRs used in this study.

cargos into the cytosol of live cells remains an unrealized milestone toward the translation of NP-based therapeutic and diagnostic tools into the clinic. Thus, exploring new strategies that can enhance uptake of gold nanomaterials, shorten the required incubation time and concentration used, while reducing endosomal sequestration (the hallmark of endocytic delivery) is very much needed.

In this report, we detail the use of SVS-1 peptide, a de novo designed anticancer peptide with the sequence KVKVKVKV^DPPTKVKVKV-NH₂, to facilitate the rapid and efficient delivery of gold colloids, namely, spherical nanoparticles (AuNPs) and large nanorods (AuNRs) inside HeLa cells. This peptide was designed to bind to the negatively charged surfaces of cancer cells, fold to form a hairpin structure, and induce their lytic destruction.^{35,36} However, when cells are incubated with concentrations of SVS-1 that are below its IC₅₀ (half-maximal inhibitory concentration), the peptide does not affect the cell viability. Instead, the peptide promotes entry, via a process involving membrane translocation, into the cytoplasm.³⁷ Motivated by these findings, we wanted to explore the potential of SVS-1 to mediate the rapid translocation of nanoscale gold colloids inside live cells. Several copies of the SVS-1 peptide along with several Texas-Red (TXR) dyes were conjugated to both AuNPs and AuNRs. Here, the TXR dye was introduced to allow fluorescence visualization of the nanocolloids inside the cells, since these Au nanocrystals are nonfluorescent. We have investigated the effectiveness of the SVS-1-facilitated intracellular uptake of the nanocolloids by HeLa cells, using fluorescence microscopy. We found that SVS-1 mediates rapid and pronounced uptake of AuNPs and AuNRs even at low concentrations, nanomolar for AuNPs and sub-nanomolar for AuNRs. Additionally, incubation of the cells with the nanomaterials in the presence of endocytic inhibitors indicates that the cell entry mechanism cannot be simply attributed to common endocytic pathways.

RESULTS AND DISCUSSION

Two sets of gold nanocrystals, namely, AuNPs (~10 nm in diameter) and AuNRs (109 nm × 20 nm, aspect ratio of ~5), have been used to test the capacity of the SVS-1 peptide to promote the delivery of such large colloids into live cells. We started with oleylamine-stabilized AuNPs and cetyltrimethylammonium bromide/sodium oleate (CTAB/NaOL)-stabilized AuNRs, which have been grown following literature protocols.^{5,38} Transmission electron microscopy (TEM) images of these nanocrystals are shown in Figure 1. The native ligands on the nanocrystals were exchanged with a multicoordinating polymer coating presenting several imidazole anchors along with several poly(ethylene glycol) (PEG) blocks, where a fraction of those blocks is amine-terminated (reactive), whereas the other is methoxy-terminated (inert), histamine (His)-poly(isobutylene-*alt*-maleic anhydride) (PIMA)-PEG-OCH₃/NH₂.³⁹ The use of a multidentate polymer coating instead of a monodentate ligand (e.g., monothiol-PEG) is advantageous, in particular, when colloids with large surface areas are involved, such as is the case for the AuNRs used here. Such coating also yields nanomaterials with substantially better colloidal stability and reduced nonspecific interactions.^{40,41} The polymer presents several amines per ligand, which allows for the simultaneous conjugation of multiple peptides and other functionalities to a nanocrystal. We estimate that based on the ligand structure, size of the nanocrystal, and the fraction of PEG-NH₂ blocks inserted in a ligand, there are ~4000 amines per AuNR and ~170 amines per AuNP.⁴² Approximately, 50% of the available amine groups was functionalized with maleimide using *N*-hydroxysuccinamide-3-(3-methyl-2,5-mioxo-2,5-dihydro-1*H*-pyrrol-1-yl)-propionic acid (NHS-ester maleimide). The maleimide groups were then coupled to the N-terminal cysteine of a modified SVS-1 peptide (CGGKVKVVKV^DPPTKVKVKV-NH₂), which forms a stable thioether linkage between the nanocrystal and the peptide (see Figure 1A).⁴³ The remaining fraction of

amines was coupled to Texas-Red NHS ester, to afford fluorescence tracking of the conjugated AuNPs and AuNRs. The absorption and emission profiles of the TXR-labeled AuNP-SVS-1 and AuNR-SVS-1 conjugates are shown in Figure 2. The emission profiles fall largely outside the absorption

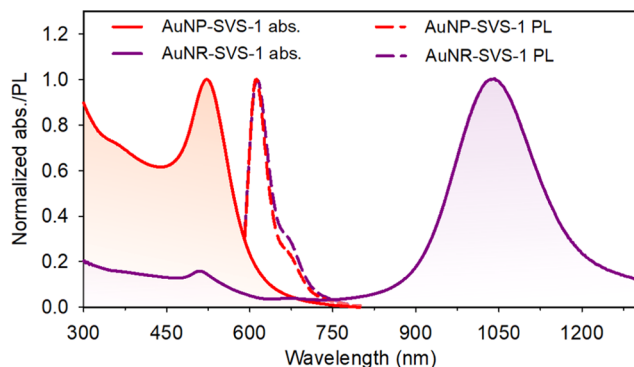


Figure 2. Absorption and emission spectra (normalized with respect to the peak values) collected from TXR-labeled AuNP-SVS-1 and AuNR-SVS-1 dispersions. Samples were excited at 580 nm. Note that the dye contribution to the AuNP or AuNR absorption (over the range 550–600 nm) is very small (essentially negligible), a property that can be largely attributed to the very large extinction coefficient of the metal nanocolloids compared to that of TXR.

ranges (bands) of both colloids. In addition, rather large photoluminescence intensities are generated from these dispersions, which is a direct result of coupling large numbers of TXR per nanocrystal; this allows one to circumvent (and reduce) the effects of fluorescence quenching of dye emission by proximal metallic nanostructures.⁴⁴ Additional details on the ligand exchange and conjugate preparation are provided in the [Experimental Section](#).

The effectiveness of the SVS-1 peptide to facilitate intracellular delivery of AuNPs and AuNRs into live cells was first tested by incubating the colloid conjugates with eukaryotic mammalian HeLa cells at different concentrations for 1 h at 37 °C. The set of panels in Figure 3 shows epifluorescence images collected from cells incubated with AuNP-SVS-1/TXR conjugates at different concentrations (2, 4, and 5 nM with respect to AuNPs). Shown are differential interference contrast (DIC) images of the cell morphology, blue 4',6-diamidino-2-phenylindole (DAPI) staining of the nuclei, red fluorescence of the TXR dye (i.e., AuNP-conjugates), along with the merged fluorescence images. Figure 4 shows images for cell cultures incubated with AuNR-SVS-1/TXR conjugates (at 0.1, 0.2, and 0.3 nM with respect to AuNRs), namely, DIC images, epifluorescence of the DAPI-stained nuclei (blue), red staining ascribed to the AuNP-TXR emission, together with the merged images (right panels). Two sets of control experiments probing cellular uptake of the AuNPs and AuNRs in the absence of peptides were also carried out. In the first set, the cells were incubated with dye-labeled nanocolloids (i.e., no SVS-1), AuNP-TXR at 5 nM and AuNR-TXR at 0.3 nM. The second set probed the cellular uptake of pure AuNP/AuNRs (i.e., nanocolloids in the absence of SVS-1 and TXR) using 5 nM of AuNPs and 0.3 nM of AuNRs.

For both sets of conjugates, the collected images show that significant levels of uptake are observed even at the lowest concentrations used for SVS-1-conjugated AuNPs and AuNRs

(2 nM for AuNPs and 0.1 nM for AuNRs). Furthermore, the images show a homogeneous red staining across the cell volumes excluding the nuclei; this suggests that following uptake the conjugates do not penetrate the cell nucleus. In comparison, images collected from control experiments clearly show that no internalization was measured for cells exposed to dispersions of nanocrystals alone (no TXR and no peptide) or TXR-labeled nanocrystals (AuNP-TXR or AuNR-TXR). The pronounced uptake of only peptide-coupled nanocrystals proves the effectiveness of SVS-1 in delivering AuNPs or AuNRs into live cells; notably a pronounced uptake was measured at sub-nanomolar concentrations for AuNR-conjugates. The pronounced uptake is likely due to an increased number of peptides per nanocrystal-SVS-1 conjugate (i.e., high valence), which is facilitated by the high number of amine groups presented on the AuNPs/AuNRs. The latter results from a combination of large surface areas of the colloids and the ability to tune the ligand stoichiometry.³⁹ For instance, the AuNPs and AuNRs have substantially larger surface areas than luminescent quantum dots, whereas the polymer presents ~6 amines per ligand.⁴⁵ We anticipate based on the number of amine groups per nanocrystals that there are up to ~80 SVS-1 per AuNP- and over ~1000 peptide per AuNR-conjugate, if we assume that approx. half of the amine groups has been coupled to peptides.

The above results combined indicate that the SVS-1 peptide is very effective in delivering the Au nanocrystals into live cells. Additionally, the red staining of the TXR-labeled AuNP-SVS-1 or AuNR-SVS-1 conjugates is homogenous, suggesting that endocytosis may not be a dominant mechanism in their uptake. To identify whether or not the observed peptide-mediated uptake of the AuNPs and AuNRs is promoted by endocytic pathways, additional internalization studies were conducted in the presence of three common physiological and pharmacological inhibitors of endocytosis. First, the temperature of the cell culture was maintained at 4 °C for 40 min to halt endocytic activity in the cells, followed by incubation with the AuNP-SVS-1 or AuNR-SVS-1 conjugates for another 40 min. This experiment allowed us to test the effects of reducing all cells activities, including metabolic activities and endocytosis, which is expected to occur when the temperature of the cultures is lowered from 37 to 4 °C, eliminating endocytosis as an uptake process.^{46,47} The cells were fixed and then imaged using epifluorescence microscopy. In the second set of experiments, we tested the effects of introducing two chemical inhibitors of endocytotic uptake. In one experiment, the cultures were first pretreated with sodium azide (NaN₃, 10 mM) and 2-deoxy-D-glucose (50 mM) for 30 min, followed by incubation with AuNP-SVS-1 or AuNR-SVS-1 conjugates for 40 min, and then imaged. In the other experiment, the cells were initially incubated with a hypertonic sucrose solution (0.4 M) for 1 h, then with the conjugates for 40 min, followed by fluorescence imaging. Incubation with 2-deoxy-D-glucose and NaN₃ is expected to inhibit glycolysis and mitochondrial oxidative phosphorylation, respectively, which leads to impairment of adenosine triphosphate (ATP) production (thus altering the active process of endocytosis).³⁷ Conversely, exposing the cell culture to a hypertonic sucrose solution specifically inhibits the clathrin-mediated endocytosis.^{48–50} The panels shown in Figure 5A,B indicate that significant red staining from the AuNP- and AuNR-conjugates is still measured inside the cells under all three endocytosis inhibition conditions tested. These results suggest that inhibiting

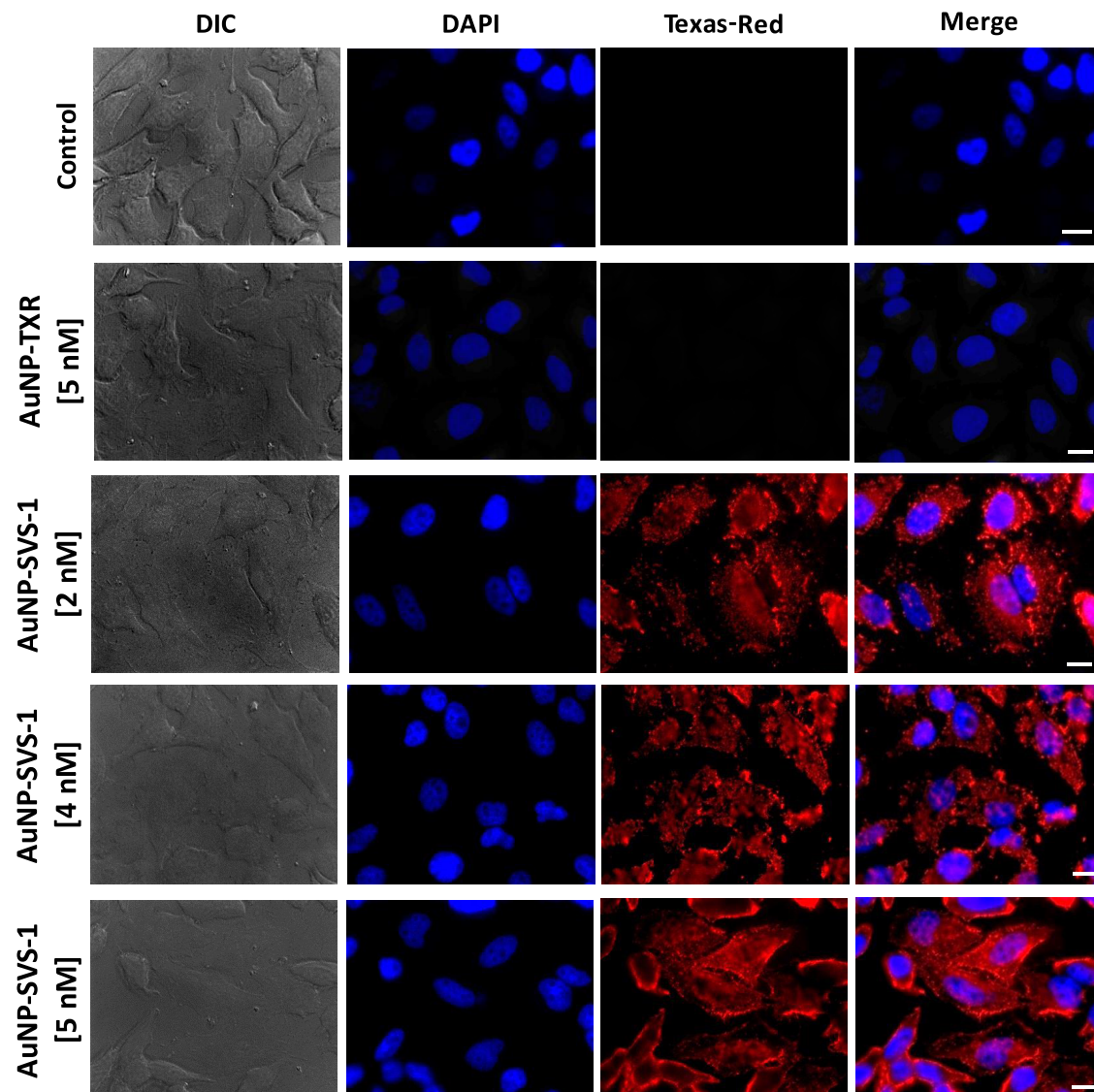


Figure 3. SVS-1-mediated intracellular delivery of AuNP-conjugates into HeLa cells. Shown are the (DIC), DAPI (nuclei), Texas-Red and merged DAPI (nuclei) and Texas-Red epifluorescence images of control cells and cells incubated with varying concentrations of nanoconjugates of AuNP-TXR (5 nM) and AuNP-SVS-1 (2–5 nM) for 1 h at 37 °C. The Texas-Red dye coupled to AuNP-conjugates allowed visualization of the Au nanocrystal distribution inside the cells. Scale bar $\sim 10 \mu\text{m}$.

endocytosis (by reducing all cell activities, ATP-depletion, and blocking clathrin-mediated uptake) has little to no effect on the levels of cell staining facilitated by decorating the AuNPs and AuNRs with several copies of SVS-1. They also agree with previous findings, which have indicated that incubating cells with SVS-1 at subtoxic concentrations promotes uptake of the peptide into cells via primarily physical translocative mechanisms.³⁶ This peptide is thus potentially promising and should be further explored as a means of delivering various nanomaterials inside live cells, likely via membrane translocation.

We would like to stress that incubation of the HeLa cells with the gold nanocolloids while yielding high levels of staining across the cell volume (excluding the nucleus), it did not alter the viability of the cell culture as confirmed using 3-(4,5-dimethylthiazol-2-yl)-2,5-diphenyltetrazolium bromide (MTT) assay. The cells were first incubated with the nanocolloids for 24 h at concentrations ranging from 0.25 to 4 nM for AuNP-SVS-1 (or AuNPs) and from 0.0125 to 0.2 nM for AuNRs or

AuNP-SVS-1 conjugates. After that the cultures were incubated with MTT for 3 h, and then dimethyl sulfoxide (DMSO) was added followed by collection of the absorption data. The viability data reported in Figure 6 clearly show that no changes in the fraction of healthy cells are measured over the range of concentrations tested. Combined with the intact morphology of the cells shown in the DIC images (Figures 3 and 4), these viability data indicate that the presence of either set of conjugates does not induce any measurable changes in the cell health or functions. This result is consistent with previous findings reported in reference,³⁶ where it was shown that incubation of cells with pure SVS-1 at concentration smaller than IC_{50} value did not affect the cell viability.

CONCLUSIONS

We have tested the capacity of a lysine-rich 18 amino acid peptide, SVS-1, initially designed as an anticancer peptide, to deliver AuNPs and AuNRs into live mammalian cells, via potentially direct translocation through the plasma membrane.

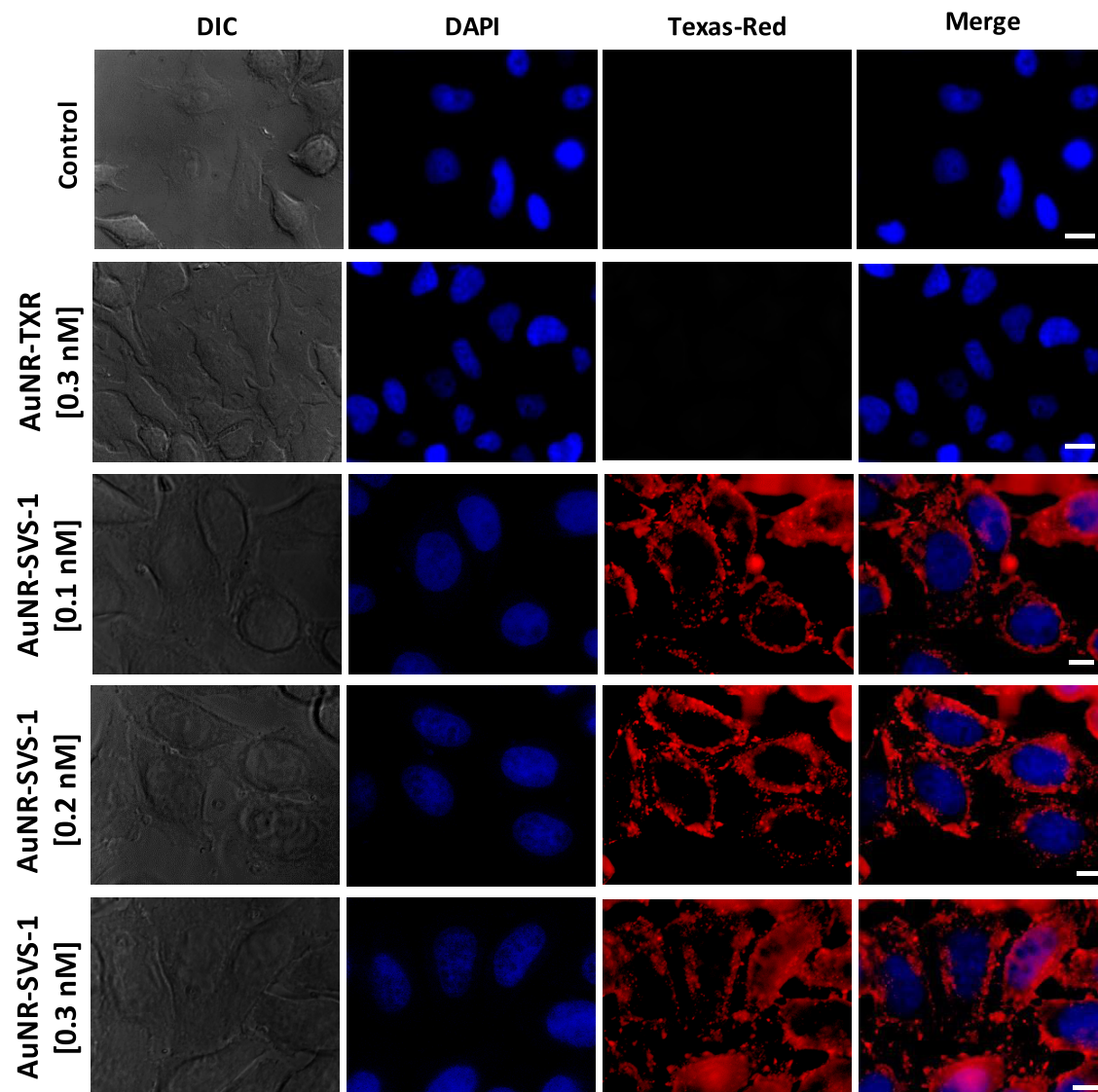


Figure 4. SVS-1-mediated intracellular delivery of AuNR-conjugates into HeLa cells. Shown are the (DIC), DAPI (nuclei), Texas-Red and merged DAPI (nuclei) and Texas-Red epifluorescence images of control cells and cells incubated with varying concentrations of nanoconjugates of AuNR-TXR (0.3 nM) and AuNR-SVS-1 (0.1–0.3 nM) for 1 h at 37 °C. The Texas-Red dye allowed visualization of the Au nanocrystal distribution inside the cells. Scale bar ~ 10 μ m.

Our results combining fluorescence imaging and endocytosis inhibition measurements indicate that this membrane-active peptide can promote a pronounced intracellular delivery of AuNPs and AuNRs. We found that delivery of both cargos is not affected by conjugate concentration, implying that uptake is rapid. Moreover, uptake of both sets of nanomaterials persists under inhibition conditions that drastically limit endocytosis. This strongly suggests a mechanism of cell entry that involves direct translocation across the membrane. These findings are promising and indicate that SVS-1 (and its derivatives) could address the limitations currently encountered in delivering various nanomaterials into live cells. Our approach offers a direct and more effective strategy for the intracellular delivery of nanoconjugates than other routes that rely on endocytic uptake, followed by endosome/lysosome disruption to access the cytoplasm. These approaches tend to release the content of those endo/lysosomes in the cytosol, which may negatively affect the cell health. Furthermore, our findings may open up new opportunities for intracellular

biosensing applications using high-resolution TEM imaging of cells treated with peptide-functionalized nanocrystals, given the high electronic contrast offered by the Au cores. We are presently testing this approach and hope to report on our findings in the future.

EXPERIMENTAL SECTION

Solid-Phase Peptide Synthesis. The cysteine-modified SVS-1 peptide with the sequence CGGKVKVKV^DPPTKVKVKV-NH₂ was synthesized on PL-Rink resin using an automated ABI 433A peptide synthesizer via fluorenylmethoxycarbonyl-based solid-phase peptide chemistry with HCTU activation. The peptide was cleaved from the resin and deprotected under argon atmosphere using a trifluoroacetic acid (TFA)/thioanisole/1,2-ethanedithiol/anisole (90:5:3:2) mixture for 2 h. The crude product was precipitated with cold diethyl ether and lyophilized. Purification of the compound relied on reverse-phase high-performance liquid chromatography (HPLC) using

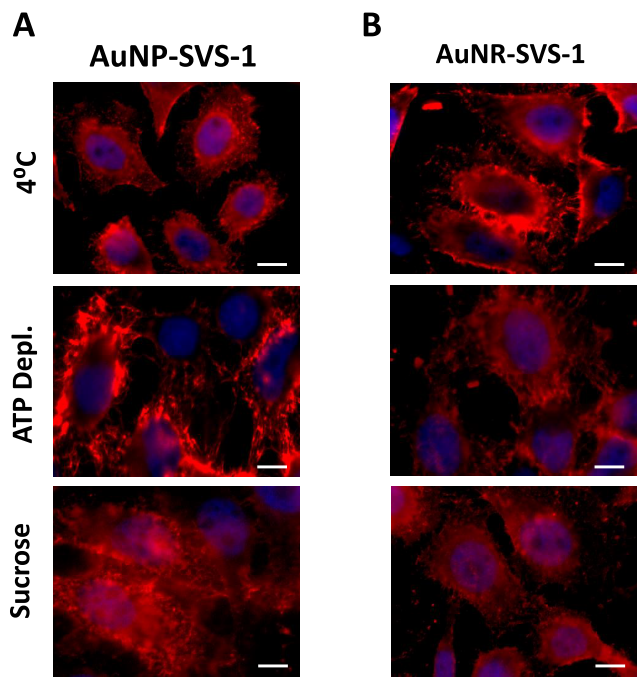


Figure 5. Endocytosis inhibition experiments. (A, B) Representative fluorescence images of HeLa cells incubated with AuNP-SVS-1 (2 nM) and AuNR-SVS-1 (0.2 nM) conjugates for 40 min at 4 °C (top panels), in the presence of sodium azide (middle panels) and in the presence hypertonic sucrose solution (bottom panels). The cell nuclei were DAPI stained. Scale bar $\sim 10 \mu\text{m}$.

a system equipped with a semipreparative Vydac C18 column. A solvent mixture made of A (0.1% TFA in water) and B (0.1% TFA in 9:1 acetonitrile/water) was used for HPLC purification, with a linear gradient of 0–100% solvent B applied over 100 min. The solution was then lyophilized, yielding the product, and the purity was verified by analytical HPLC-mass spectrometry.

Polymer Ligand Synthesis. The precursors, including $\text{H}_2\text{N}-\text{PEG}_{750}-\text{OCH}_3$ and $\text{H}_2\text{N}-\text{PEG}_{600}-\text{NH}_2$, used for synthesizing the polymers were prepared in our laboratory following the procedures described in previous publications.^{51,52} The $\text{H}_2\text{N}-\text{PEG}_{600}-\text{NH}(\text{Boc})$ precursor was prepared from $\text{H}_2\text{N}-\text{PEG}_{600}-\text{NH}_2$ by reacting one amine with Boc_2O , following the protocol reported in reference.⁵³ The amine-functionalized polymer, His-PIMA-PEG-OCH₃/NH₂ (50% His, 35% PEG-OCH₃ and 15% PEG-NH₂), was prepared following the protocol reported in our recent work.³⁹ Briefly, 0.1 g of poly(isobutylene-*alt*-maleic anhydride), PIMA, was dissolved in 5 mL of DMF and added to a 25 mL three-neck round-bottom flask. The solution was purged with nitrogen and heated to 40 °C using an oil bath. Histamine (0.036 g) dissolved in DMF (1 mL) was added dropwise to the PIMA solution through a syringe, followed by addition of a DMF solution (2 mL) containing $\text{H}_2\text{N}-\text{PEG}_{750}-\text{OCH}_3$ (0.17 g) and $\text{H}_2\text{N}-\text{PEG}_{600}-\text{NH}(\text{Boc})$ (0.067 g). The reaction mixture was stirred overnight at 40 °C, and then the solvent was removed under vacuum. The residual product was dissolved in tetrahydrofuran (5 mL) followed by addition of HCl solution (0.5 mL, 4 M in dioxane) for Boc-deprotection. The mixture was stirred for 1 h at room temperature, and then the solvents were removed under vacuum. The polymer was dissolved in methanol, to which a solution of NaOH in methanol (0.1 g/mL) was added dropwise to neutralize the

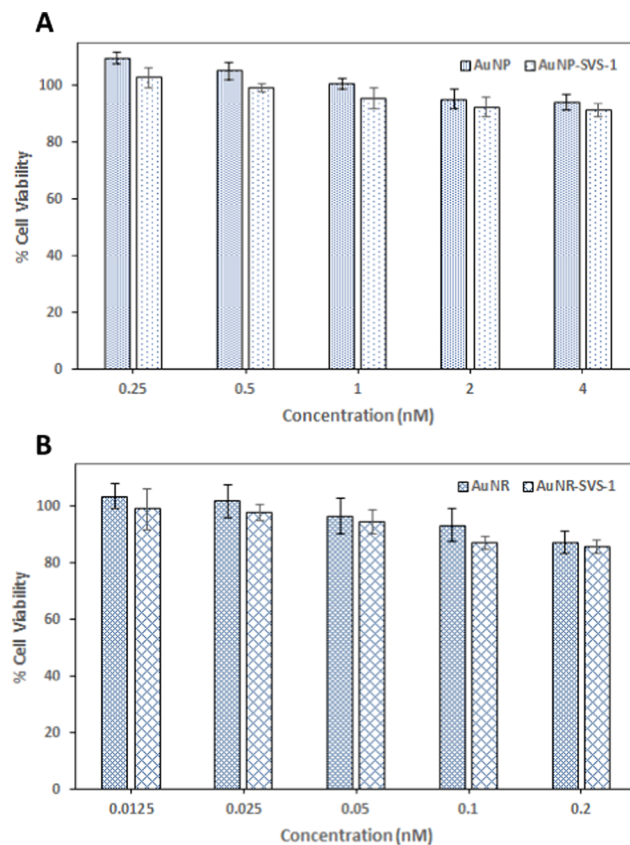


Figure 6. MTT viability assay performed on HeLa cell cultures incubated for 24 h at 37 °C with varying concentrations of AuNPs and AuNP-SVS-1 conjugates (A); AuNRs and AuNR-SVS-1 conjugates (B).

acid. The solvent was removed under vacuum, and then 5 mL of chloroform was added to precipitate the salts. One round of centrifugation was applied to remove the salts, followed by solvent removal under vacuum to yield the final His-PIMA-OCH₃/NH₂ polymer.

AuNP and AuNR Growth and Ligand Exchange. The starting oleylamine-capped AuNPs (~ 10 nm in diameter) were synthesized following the protocol described previously in reference.³⁸ For ligand exchange, 300 μL of oleylamine-capped AuNPs dispersed in hexane were precipitated with ethanol, and the precipitate was resuspended in 300 μL of CHCl₃. Separately, a ligand solution was prepared by dissolving His-PIMA-PEG-OCH₃/NH₂ (15 mg) in 300 μL of CHCl₃ and then added to the AuNP dispersion. The mixture was left stirring overnight at 50 °C. The AuNPs were precipitated with excess hexane and then pelleted by centrifugation for 5 min at 3600 rpm. This step was repeated one more time, and the AuNPs were dried under vacuum, redispersed in deionized (DI) water, and then passed through a 0.45 μm syringe filter (Millipore, Billerica, MA). Further purification to remove excess polymer ligands was carried out by applying three rounds of concentration/dilution using a centrifugal membrane filtration device (MW cutoff = 50 kDa). The final concentration of the AuNP dispersion was determined from the absorbance value at 520 nm using an extinction coefficient of $9.55 \times 10^7 \text{ M}^{-1}\text{cm}^{-1}$.^{3,54}

The gold nanorods (109 nm \times 20 nm) were prepared by seeded growth in a surfactant mixture containing hexadecyltrimethylammonium bromide (CTAB) and sodium oleate

(NaOL), following the strategy developed by Murray and co-workers.⁵ Ligand exchange of CTAB/NaOL-coated AuNRs with His-PIMA-PEG-OCH₃/NH₂ was performed in aqueous phase. AuNR stock dispersion (300 μ L, ~3 nM) was centrifuged at 7000 rpm for 5 min to remove excess CTAB and NaOL, and the pellet was resuspended in 300 μ L of DI water. Subsequently, 15 mg of His-PIMA-PEG-OCH₃/NH₂ dissolved in 500 μ L of phosphate buffer (pH 8) was added to the AuNR dispersion, and the mixture was stirred overnight at 50 °C. The aqueous solution was then passed through a 0.45 μ m syringe filter (Millipore, Billerica, MA), and excess ligand was removed by applying two rounds of concentration/dilution using a centrifugal membrane filtration device as described above. The final concentration of the AuNR dispersion was determined from the absorbance value at 1034 nm using an extinction coefficient of 7.8×10^9 M⁻¹cm⁻¹.^{23,55}

Preparation of AuNP-SVS-1/Texas-Red Conjugates

(AuNP-SVS-1/TXR). In a typical preparation, 0.046 mg of SVS-1 peptide, containing a CGG motif at its N-terminus to allow for thiol-mediated conjugation, was dissolved in 150 μ L of Tris-buffered saline (TBS) (pH 7.3) and mixed with 2 μ L of 6.98 mM solution of tris(2-carboxyethyl)phosphine (TCEP); the TCEP-to-peptide molar ratio was ~0.5. This mixture was stirred for 15 min at room temperature. In a separate glass vial, 150 μ L of ligand-exchanged AuNPs (0.22 μ M) were dispersed in 200 μ L of phosphate buffer (pH 7.5, 20 mM). To this, a mixture of 1.5 μ L of 7.1 mM NHS ester maleimide solution (in DMSO) and 58 μ L of 265 μ M NHS-ester Texas-Red (in DMSO) was added. The reaction mixture was stirred for ~30 min at room temperature after which excess NHS ester maleimide and dye were removed by applying one round of dilution/concentration with TBS (pH 7.3) using a membrane filtration device (MW cutoff = 50 kDa). The purified AuNP-TXR/maleimide dispersion was added to the peptide-TCEP mixture, and the final volume was adjusted to 400 μ L with TBS (pH 7.3). The solution was incubated for another ~3 h at room temperature while stirring. The AuNP-SVS-1/TXR conjugates were separated from byproducts and unbound peptide via size-exclusion chromatography using a PD-10 column. The conjugates were stored at 4 °C until further use.

Preparation of AuNR-SVS-1/Texas-Red Conjugates

(AuNR-SVS-1/TXR). We follow the same steps described above to prepare the AuNR-SVS-1/TXR conjugates. Briefly, SVS-1 peptide (0.1 mg) was dissolved in 150 μ L of TBS (pH 7.3) and mixed with 3 μ L of 6.98 mM TCEP (TCEP-to-peptide molar ratio ~0.5), and the mixture was stirred for 15 min at room temperature. In a separate glass vial, 200 μ L of ligand-exchanged AuNRs (5.8 nM) was dispersed in 300 μ L of phosphate buffer (pH 7.5, 20 mM). A mixture made of 6.5 μ L of 7.1 mM NHS ester maleimide solution (in DMSO) and 175 μ L of 265 μ M NHS-ester Texas-Red (in DMSO) was added. The reaction mixture was stirred for ~30 min at room temperature followed by removal of excess NHS-ester maleimide and dye by applying one round of dilution/concentration with TBS (pH 7.3) as done above. The purified AuNR-TXR-maleimide dispersion was added to the peptide-TCEP solution, and the volume was adjusted to 400 μ L by adding TBS (pH 7.3). The mixture was reacted for another ~3 h at room temperature. The AuNR-SVS-1/TXR conjugates were purified from byproducts and unbound peptide via size-exclusion chromatography using a PD-10 column. The conjugates were stored at 4 °C until further use.

Cell Culture and Inhibition Experiments. Human cervical carcinoma (HeLa) cells were acquired from the Florida State University cell culture facility. The cell cultures were grown at 37 °C under humidified 5% CO₂ atmosphere in complete growth medium (Dulbecco's modified Eagle medium, DMEM) supplemented with 10% (v/v) fetal bovine serum, L-glutamine, sodium pyruvate, 1% (v/v) antibiotic-antimycotic 100X, and 1% (v/v) nonessential amino acid solution 100X. For incubation experiments, 7×10^4 cells were seeded onto 12 mm round microcover glasses in a 24-well microplate (CellStar, VWR), and then incubated overnight to allow for cell attachment. For uptake studies, the cell cultures were incubated with dispersions of the nanocrystal-TXR or nanocrystal-SVS-1/TXR conjugates, prepared in serum-free DMEM media at the desired concentrations. After incubation, the cells were washed three times with TBS buffer, fixed with 3.7% paraformaldehyde, and then stained with DAPI to visualize the nuclei.

The endocytosis inhibition experiments were carried out using cells, which have been cultured overnight in 24-well microplate as done above. Three sets of inhibition experiments were carried out. (1) The cell cultures were preincubated at 4 °C for 40 min prior to mixing with the AuNP/NR-conjugates.⁴⁷ (2) ATP-depletion experiments were carried out by preincubating the cells in glucose and serum-free media containing 10 mM sodium azide and 50 mM 2-deoxy-D-glucose for 30 min prior to exposure to AuNP/NR-conjugates.⁵⁶ (3) The cells were preincubated in serum-free media containing 0.45 M sucrose for 1 h; this is expected to selectively prevent uptake promoted by clathrin-mediated endocytosis.⁵⁷ The pretreated cells were washed with serum-free media followed by incubation with the conjugates at the required concentrations for 40 min. The cultures were then washed, fixed, and stained with DAPI, as described above.

Fluorescence Imaging Experiments. An Inverted Nikon Eclipse Ti Microscope equipped with a color CoolSNAP HQ2 CCD camera (available at the FSU Department of Chemistry) was utilized to collect the fluorescence images of the various labeled and fixed cell cultures. Excitation of the cultures was provided by a Xe lamp, whereas the fluorescence images were collected using a 60X objective (Nikon) and a set of filter cubes (Chroma Technology, Rockingham, VT). These include a DAPI cube (with 340–380 nm excitation and 435–485 nm emission) to visualize the nuclei and a Texas-Red HYQ cube (with 532–587 nm excitation and 608–683 nm emission) for visualization of the AuNP-SVS-1/TXR and AuNR-SVS-1/TXR conjugates.

ASSOCIATED CONTENT

Supporting Information

The Supporting Information is available free of charge on the ACS Publications website at DOI: [10.1021/acsomega.8b02276](https://doi.org/10.1021/acsomega.8b02276).

Materials, characterization, and cell viability assay (PDF)

AUTHOR INFORMATION

ORCID

Scott H. Medina: [0000-0001-5441-2164](https://orcid.org/0000-0001-5441-2164)

Wentao Wang: [0000-0003-2273-4171](https://orcid.org/0000-0003-2273-4171)

Hedi Mattoussi: [0000-0002-6511-9323](https://orcid.org/0000-0002-6511-9323)

Present Addresses

¹The Food and Drug Administration, National Center for Toxicological Research, 3900 NCTR Road, Jefferson, Arkansas 72079, United States (G.P.).

²DNA Electronics, Inc., 1891 Rutherford Road, Suite 100, Carlsbad, California 92008, United States (W.W.).

³Department of Biomedical Engineering, Pennsylvania State University, University Park, State College, Pennsylvania 16802, United States (S.H.M.).

Notes

The authors declare no competing financial interest.

ACKNOWLEDGMENTS

This work was supported by the National Science Foundation (NSF-CHE #1508501), National Institutes of Health (NIH #R01 DC013080), Asahi-Kasei Corp., and the Intramural Research Program of the National Cancer Institute (National Institutes of Health, Project #BC011313).

REFERENCES

- (1) Brust, M.; Walker, M.; Bethell, D.; Schiffrin, D. J.; Whyman, R. Synthesis of thiol-derivatized gold nanoparticles in a 2-phase liquid-liquid system. *J. Chem. Soc., Chem. Commun.* **1994**, 801–802.
- (2) Jana, N. R.; Gearheart, L.; Murphy, C. J. Wet Chemical Synthesis of High Aspect Ratio Cylindrical Gold Nanorods. *J. Phys. Chem. B* **2001**, *105*, 4065–4067.
- (3) Oh, E.; Susumu, K.; Goswami, R.; Matoussi, H. One-Phase Synthesis of Water-Soluble Gold Nanoparticles with Control over Size and Surface Functionalities. *Langmuir* **2010**, *26*, 7604–7613.
- (4) Dreden, E. C.; Alkilany, A. M.; Huang, X.; Murphy, C. J.; El-Sayed, M. A. The golden age: gold nanoparticles for biomedicine. *Chem. Soc. Rev.* **2012**, *41*, 2740–2779.
- (5) Ye, X.; Zheng, C.; Chen, J.; Gao, Y.; Murray, C. B. Using Binary Surfactant Mixtures To Simultaneously Improve the Dimensional Tunability and Monodispersity in the Seeded Growth of Gold Nanorods. *Nano Lett.* **2013**, *13*, 765–771.
- (6) Link, S.; Mohamed, M. B.; El-Sayed, M. A. Simulation of the Optical Absorption Spectra of Gold Nanorods as a Function of Their Aspect Ratio and the Effect of the Medium Dielectric Constant. *J. Phys. Chem. B* **1999**, *103*, 3073–3077.
- (7) Pérez-Juste, J.; Pastoriza-Santos, I.; Liz-Marzán, L. M.; Mulvaney, P. Gold nanorods: Synthesis, characterization and applications. *Coord. Chem. Rev.* **2005**, *249*, 1870–1901.
- (8) Alkilany, A. M.; Lohse, S. E.; Murphy, C. J. The Gold Standard: Gold Nanoparticle Libraries To Understand the Nano-Bio Interface. *Acc. Chem. Res.* **2013**, *46*, 650–661.
- (9) Saha, K.; Agasti, S. S.; Kim, C.; Li, X. N.; Rotello, V. M. Gold Nanoparticles in Chemical and Biological Sensing. *Chem. Rev.* **2012**, *112*, 2739–2779.
- (10) Howes, P. D.; Chandrawati, R.; Stevens, M. M. Colloidal nanoparticles as advanced biological sensors. *Science* **2014**, *346*, No. 1247390.
- (11) Palui, G.; Aldeek, F.; Wang, W.; Matoussi, H. Strategies for interfacing inorganic nanocrystals with biological systems based on polymer-coating. *Chem. Soc. Rev.* **2015**, *44*, 193–227.
- (12) Zhou, W.; Gao, X.; Liu, D.; Chen, X. Gold Nanoparticles for In Vitro Diagnostics. *Chem. Rev.* **2015**, *115*, 10575–10636.
- (13) Melamed, J. R.; Riley, R. S.; Valcourt, D. M.; Day, E. S. Using Gold Nanoparticles To Disrupt the Tumor Microenvironment: An Emerging Therapeutic Strategy. *ACS Nano* **2016**, *10*, 10631–10635.
- (14) Ding, Y.; Jiang, Z.; Saha, K.; Kim, C. S.; Kim, S. T.; Landis, R. F.; Rotello, V. M. Gold Nanoparticles for Nucleic Acid Delivery. *Mol. Ther.* **2014**, *22*, 1075–1083.
- (15) Saha, K.; Kim, S. T.; Yan, B.; Miranda, O. R.; Alfonso, F. S.; Shlosman, D.; Rotello, V. M. Surface Functionality of Nanoparticles Determines Cellular Uptake Mechanisms in Mammalian Cells. *Small* **2013**, *9*, 300–305.
- (16) Jiang, Y.; Huo, S.; Mizuhara, T.; Das, R.; Lee, Y.-W.; Hou, S.; Moyano, D. F.; Duncan, B.; Liang, X.-J.; Rotello, V. M. The Interplay of Size and Surface Functionality on the Cellular Uptake of Sub-10 nm Gold Nanoparticles. *ACS Nano* **2015**, *9*, 9986–9993.
- (17) Nativo, P.; Prior, I. A.; Brust, M. Uptake and Intracellular Fate of Surface-Modified Gold Nanoparticles. *ACS Nano* **2008**, *2*, 1639–1644.
- (18) Li Volsi, A.; Scialabba, C.; Vetri, V.; Cavallaro, G.; Licciardi, M.; Giammona, G. Near-Infrared Light Responsive Folate Targeted Gold Nanorods for Combined Photothermal-Chemotherapy of Osteosarcoma. *ACS Appl. Mater. Interfaces* **2017**, *9*, 14453–14469.
- (19) El-Sayed, I. H.; Huang, X.; El-Sayed, M. A. Selective laser photo-thermal therapy of epithelial carcinoma using anti-EGFR antibody conjugated gold nanoparticles. *Cancer Lett.* **2006**, *239*, 129–135.
- (20) Huang, X.; El-Sayed, I. H.; Qian, W.; El-Sayed, M. A. Cancer cell imaging and photothermal therapy in the near-infrared region by using gold nanorods. *J. Am. Chem. Soc.* **2006**, *128*, 2115–2120.
- (21) Alkilany, A. M.; Thompson, L. B.; Boulos, S. P.; Sisco, P. N.; Murphy, C. J. Gold nanorods: Their potential for photothermal therapeutics and drug delivery, tempered by the complexity of their biological interactions. *Adv. Drug Delivery Rev.* **2012**, *64*, 190–199.
- (22) Du, Y. Q.; Yang, X. X.; Li, W. L.; Wang, J.; Huang, C. Z. A cancer-targeted drug delivery system developed with gold nanoparticle mediated DNA-doxorubicin conjugates. *RSC Adv.* **2014**, *4*, 34830–34835.
- (23) Jain, P. K.; Lee, K. S.; El-Sayed, I. H.; El-Sayed, M. A. Calculated Absorption and Scattering Properties of Gold Nanoparticles of Different Size, Shape, and Composition: Applications in Biological Imaging and Biomedicine. *J. Phys. Chem. B* **2006**, *110*, 7238–7248.
- (24) Cole, L. E.; Ross, R. D.; Tilley, J. M.; Vargo-Gogola, T.; Roeder, R. K. Gold nanoparticles as contrast agents in x-ray imaging and computed tomography. *Nanomedicine* **2015**, *10*, 321–341.
- (25) Tong, L.; Wei, Q.; Wei, A.; Cheng, J. X. Gold nanorods as contrast agents for biological imaging: optical properties, surface conjugation and photothermal effects. *Photochem. Photobiol.* **2009**, *85*, 21–32.
- (26) Gao, F.; Bai, L.; Liu, S.; Zhang, R.; Zhang, J.; Feng, X.; Zheng, Y.; Zhao, Y. Rationally encapsulated gold nanorods improving both linear and nonlinear photoacoustic imaging contrast in vivo. *Nanoscale* **2017**, *9*, 79–86.
- (27) Chithrani, B. D.; Ghazani, A. A.; Chan, W. C. W. Determining the size and shape dependence of gold nanoparticle uptake into mammalian cells. *Nano Lett.* **2006**, *6*, 662–668.
- (28) Chithrani, B. D.; Chan, W. C. W. Elucidating the Mechanism of Cellular Uptake and Removal of Protein-Coated Gold Nanoparticles of Different Sizes and Shapes. *Nano Lett.* **2007**, *7*, 1542–1550.
- (29) Verma, A.; Uzun, O.; Hu, Y.; Hu, Y.; Han, H.-S.; Watson, N.; Chen, S.; Irvine, D. J.; Stellacci, F. Surface-structure-regulated cell-membrane penetration by monolayer-protected nanoparticles. *Nat. Mater.* **2008**, *7*, 588.
- (30) Dykman, L. A.; Khlebtsov, N. G. Uptake of Engineered Gold Nanoparticles into Mammalian Cells. *Chem. Rev.* **2014**, *114*, 1258–1288.
- (31) Tkachenko, A. G.; Xie, H.; Liu, Y.; Coleman, D.; Ryan, J.; Glomm, W. R.; Shipton, M. K.; Franzen, S.; Feldheim, D. L. Cellular Trajectories of Peptide-Modified Gold Particle Complexes: Comparison of Nuclear Localization Signals and Peptide Transduction Domains. *Bioconjugate Chem.* **2004**, *15*, 482–490.
- (32) Alkilany, A. M.; Murphy, C. J. Toxicity and cellular uptake of gold nanoparticles: what we have learned so far? *J. Nanopart. Res.* **2010**, *12*, 2313–2333.
- (33) Shukla, R.; Bansal, V.; Chaudhary, M.; Basu, A.; Bhonde, R. R.; Sastry, M. Biocompatibility of Gold Nanoparticles and Their Endocytotic Fate Inside the Cellular Compartment: A Microscopic Overview. *Langmuir* **2005**, *21*, 10644–10654.

(34) Jiang, W.; Kim, B. Y. S.; Rutka, J. T.; Chan, W. C. W. Nanoparticle-mediated cellular response is size-dependent. *Nat. Nanotechnol.* **2008**, *3*, 145.

(35) Gaspar, D.; Veiga, A. S.; Sinthuvanich, C.; Schneider, J. P.; Castanho, M. A. R. B. Anticancer Peptide SVS-1: Efficacy Precedes Membrane Neutralization. *Biochemistry* **2012**, *51*, 6263–6265.

(36) Sinthuvanich, C.; Veiga, A. S.; Gupta, K.; Gaspar, D.; Blumenthal, R.; Schneider, J. P. Anticancer β -Hairpin Peptides: Membrane-Induced Folding Triggers Activity. *J. Am. Chem. Soc.* **2012**, *134*, 6210–6217.

(37) Medina, S. H.; Schneider, J. P. Cancer cell surface induced peptide folding allows intracellular translocation of drug. *J. Controlled Release* **2015**, *209*, 317–326.

(38) Liu, S.; Chen, G.; Prasad, P. N.; Swihart, M. T. Synthesis of Monodisperse Au, Ag, and Au–Ag Alloy Nanoparticles with Tunable Size and Surface Plasmon Resonance Frequency. *Chem. Mater.* **2011**, *23*, 4098–4101.

(39) Wang, W.; Kapur, A.; Ji, X.; Safi, M.; Palui, G.; Palomo, V.; Dawson, P. E.; MattoSSI, H. Photoligation of an Amphiphilic Polymer with Mixed Coordination Provides Compact and Reactive Quantum Dots. *J. Am. Chem. Soc.* **2015**, *137*, 5438–5451.

(40) Wang, W.; Aldeek, F.; Ji, X.; Zeng, B. R.; MattoSSI, H. A multifunctional amphiphilic polymer as a platform for surface-functionalizing metallic and other inorganic nanostructures. *Faraday Discuss.* **2014**, *175*, 137–151.

(41) Wang, W.; Ji, X.; Du, L.; MattoSSI, H. Enhanced Colloidal Stability of Various Gold Nanostructures Using a Multicoordinating Polymer Coating. *J. Phys. Chem. C* **2017**, *121*, 22901–22913.

(42) Wang, W.; Ji, X.; Kapur, A.; Zhang, C.; MattoSSI, H. A Multifunctional Polymer Combining the Imidazole and Zwitterion Motifs as a Biocompatible Compact Coating for Quantum Dots. *J. Am. Chem. Soc.* **2015**, *137*, 14158–14172.

(43) Hermanson, G. T. *Bioconjugate Techniques*, 3rd ed.; Academic press, 2013; pp 1–1146.

(44) Singh, M. P.; Strouse, G. F. Involvement of the LSPR Spectral Overlap for Energy Transfer between a Dye and Au Nanoparticle. *J. Am. Chem. Soc.* **2010**, *132*, 9383–9391.

(45) Zhan, N.; Palui, G.; Merkl, J.-P.; MattoSSI, H. Bio-orthogonal Coupling as a Means of Quantifying the Ligand Density on Hydrophilic Quantum Dots. *J. Am. Chem. Soc.* **2016**, *138*, 3190–3201.

(46) Delehanty, J. B.; Medintz, I. L.; Pons, T.; Brunel, F. M.; Dawson, P. E.; MattoSSI, H. Self-Assembled Quantum Dot–Peptide Bioconjugates for Selective Intracellular Delivery. *Bioconjugate Chem.* **2006**, *17*, 920–927.

(47) Jaiswal, J. K.; MattoSSI, H.; Mauro, J. M.; Simon, S. M. Long-term multiple color imaging of live cells using quantum dot bioconjugates. *Nat. Biotechnol.* **2003**, *21*, 47–51.

(48) Anas, A.; Okuda, T.; Kawashima, N.; Nakayama, K.; Itoh, T.; Ishikawa, M.; Biju, V. Clathrin-mediated endocytosis of quantum dot-peptide conjugates in living cells. *ACS Nano* **2009**, *3*, 2419–2429.

(49) Heuser, J. E.; Anderson, R. G. Hypertonic media inhibit receptor-mediated endocytosis by blocking clathrin-coated pit formation. *J. Cell Biol.* **1989**, *108*, 389–400.

(50) Daukas, G.; Zigmund, S. H. Inhibition of receptor-mediated but not fluid-phase endocytosis in polymorphonuclear leukocytes. *J. Cell Biol.* **1985**, *101*, 1673–1679.

(51) Mei, B. C.; Susumu, K.; Medintz, I. L.; MattoSSI, H. Polyethylene glycol-based bidentate ligands to enhance quantum dot and gold nanoparticle stability in biological media. *Nat. Protoc.* **2009**, *4*, 412–423.

(52) Susumu, K.; Mei, B. C.; MattoSSI, H. Multifunctional ligands based on dihydrolipoic acid and polyethylene glycol to promote biocompatibility of quantum dots. *Nat. Protoc.* **2009**, *4*, 424–436.

(53) Kaiser, K.; Marek, M.; Haselgrübler, T.; Schindler, H.; Gruber, H. J. Basic Studies on Heterobifunctional Biotin–PEG Conjugates with a 3-(4-Pyridyldithio)propionyl Marker on the Second Terminus. *Bioconjugate Chem.* **1997**, *8*, 545–551.

(54) Liu, X.; Atwater, M.; Wang, J.; Huo, Q. Extinction coefficient of gold nanoparticles with different sizes and different capping ligands. *Colloids Surf., B* **2007**, *58*, 3–7.

(55) Orendorff, C. J.; Murphy, C. J. Quantitation of Metal Content in the Silver-Assisted Growth of Gold Nanorods. *J. Phys. Chem. B* **2006**, *110*, 3990–3994.

(56) Drin, G.; Cottin, S.; Blanc, E.; Rees, A. R.; Temsamani, J. Studies on the Internalization Mechanism of Cationic Cell-penetrating Peptides. *J. Biol. Chem.* **2003**, *278*, 31192–31201.

(57) Massodi, I.; Bidwell, G. L.; Raucher, D. Evaluation of cell penetrating peptides fused to elastin-like polypeptide for drug delivery. *J. Controlled Release* **2005**, *108*, 396–408.